www.advmattechnol.de

# A Biodegradable Hybrid Micro/Nano Conductive Zinc Paste for Paper-Based Flexible Bioelectronics

Amin Zareei, Vidhya Selvamani, Sarath Gopalakrishnan, Sachin Kadian, Murali Kannan Maruthamuthu, Zihao He, Juliane Nguyen, Haiyan Wang, and Rahim Rahimi\*

Paper-based electronics are emerging as a new class of technology with broad areas of application. Despite several efforts to fabricate new types of flexible electronic devices by screen printing of conductive paste, many of them are often nonbiodegradable, toxic, and expensive, limiting their practical use in bioresorbable paper-based electronics. To address this need, a highly conductive and biodegradable bimodal conductive paste is developed using cost-effective zinc-based micro and nanoparticles with a facile low-temperature sintering process compatible with paper substrates. The two-step sintering process involves the removal of the insulating zinc oxide layer by spray coating acetic acid followed by a heat press sintering process to ensure the formation of highly packed and continuous metallic traces. The required conditions for the heat press sintering process are systematically studied using electrical, optical, and mechanical characterization techniques. The results of these investigations revealed an ultra-packed microstructure with high electrical conductivity (0.5  $\times$ 10<sup>5</sup> S m<sup>-1</sup>) and low oxide content that is obtained with a heat press sintering setting of 220 °C for 60 s. Finally, as a proof of concept, the conductive paste with an optimized sintering process is used to fabricate a wearable wireless heater for remote-controlled release of therapeutics. The controlled delivery of the system is validated in the practical and on-demand delivery of antibiotics for eradicating commonly found bacteria such as Staphylococcus aureus in dermal wound infections. The biocompatibility of all the materials and manufacturing process is validated by NIH/3T3 fibroblast cells via MTT assay and live/dead staining.

1. Introduction

In the past few years, printed electronics (PE) have gained significant attention spanning from academia to industry with

a broad spectrum of applications due to their unique characteristics such as high mechanical flexibility, low cost, and scalable manufacturing.[1-4] However, many of the materials and processes used in PE devices often depend on nonbiodegradable polymer supporting substrates (such as silicone elastomers, polyethylene terephthalate, polyimide, etc.).<sup>[5-9]</sup> Considering the widespread implementation of PE, spanning from soft robots, human-machine interface, and flexible displays to advanced healthcare and virtual reality in the near future, the buildup of discarded electronic waste (e-waste) will cause adverse environmental effects. Recently, the United Nations has reported that by 2030 e-waste will grow up to 74 million metric tons on the planet, which will demand extensive landfill space for its appropriate disposal or recycling.[10] Therefore, researchers and scientists are highly inspired to find sustainable substitutes with the desired characteristics to address the concerns mentioned above.

Recently, paper-based transient bioelectronics (PTB) composed of biodegradable materials have emerged as a new class of technology that can fully degrade to benign and environmentally safe by-products after

they have served their primary function. [i1-14] Despite the known bioresorbable characteristics of the paper substrates in PTB, the conductive traces and circuitry in these devices must be made from highly conductive and bioresorbable materials through

A. Zareei, V. Selvamani, S. Kadian, H. Wang, R. Rahimi School of Materials Engineering Purdue University West Lafayette, IN 47907, USA E-mail: rrahimi@purdue.edu

The ORCID identification number(s) for the author(s) of this article can be found under https://doi.org/10.1002/admt.202101722.

© 2022 The Authors. Advanced Materials Technologies published by Wiley-VCH GmbH. This is an open access article under the terms of the Creative Commons Attribution-NonCommercial-NoDerivs License, which permits use and distribution in any medium, provided the original work is properly cited, the use is non-commercial and no modifications or adaptations are made.

A. Zareei, V. Selvamani, S. Gopalakrishnan, S. Kadian, R. Rahimi Birck Nanotechnology Center Purdue University
West Lafayette, IN 47907, USA
S. Gopalakrishnan, Z. He, H. Wang
School of Electrical and Computer Engineering
Purdue University
West Lafayette, IN 47907, USA
M. K. Maruthamuthu, J. Nguyen
Division of Pharmacoengineering and Molecular Pharmaceutics
Eshelman School of Pharmacy

University of North Carolina at Chapel Hill

Chapel Hill, NC 27599, USA

DOI: 10.1002/admt.202101722



cost-effective and scalable processes<sup>[2]</sup> such as screen printing. In this process, conductive pastes made of metal microparticles (MPs) or nanoparticles (NPs) dispersed in a liquid vehicle (aqueous or organic) with various additives as binders are deposited onto the desired paper substrate. Among different metals, magnesium (Mg), zinc (Zn), iron (Fe), and tungsten (W) are well-known biodegradable metals with demonstrated usage in different biodegradable electronic devices.<sup>[15,16]</sup> Among these metals, Zn and its alloys generally exhibit a relatively moderate degradation rate with less harmful by-products than Fe- and Mg-based metal alloys, making it a favorable metal for many bioresorbable electronics.<sup>[17–19]</sup> Furthermore, due to its biological benefits (supports cell division, immune system, and protein synthesis), it is also used in various biodegradable implantable devices ranging from bone fixtures to wireless pressure sensors.

However, one of the main challenges of Zn-based pastes is their rapid oxidation in ambient conditions.<sup>[20]</sup> The oxide layer on the surface of the ZnMPs and ZnNPs in the printed pattern prevents close electrical contacts between the particles after printing, thus making it challenging to produce highly conductive Zn printed traces. To address this issue, many nondestructive sintering approaches, such as laser, photonic, and electrochemical sintering, have been utilized as a postprinting process for Zn based inks and pastes to remove/reduce the zinc oxide insulating barrier on the particles and weld the particles to form conductive Zn printed traces. [21-24] Although these techniques exhibited promising results in achieving good conductivity levels (e.g., 106 S m<sup>-1</sup>), they still face several drawbacks, such as low electrical stability, high production time, and incompatibility with large-scale roll-to-roll printing processes. Moreover, many previously reported conductive Zn-based pastes require a relatively thick printed layer to achieve high conductivity, leading to several processing complications such as more extended post-printing processing (e.g., drying and sintering) and low mechanical stability. Hence, a general strategy that can provide a highly conductive, biodegradable screen printable Zn-based paste that can overcome the abovementioned complications is highly desired for developing nextgeneration PTB devices. In this study, Zn MPs (ZnMPs) and Zn NPs (ZnNPs) were used to prepare a bimodal conductive bioresorbable paste which can be sintered at low temperature and yield improved conductivity of printed patterns. A complete schematic illustration of the printing process with the two-step thermo-electrochemical sintering process is shown in Figure 1. After screen printing and drying the traces, diluted acetic acid (CH3COOH:H2O, 1:5 by volume) was sprayed on the printed pattern to remove and dissolve the native oxide layer formed around ZnMPs and ZnNPs (Figure 1b). The acidic conditions encourage the self-exchange among Zn and Zn2+ at H2O/Zn interfaces between the particles, which results in the welding of particles and the formation of a conductive network. Next, a heat press process was used to ensure the formation of a continuous percolation network and a high packing density of the printed pattern through sufficient contact between the conductive fillers. In this step, the heat press process enhances the removal of the zinc oxide from the ZnMPs and ZnNPs by accelerating the rate of reaction of the acetic acid and activating the ethylene glycol (EG) reducing agents in the pastes while simultaneously applying pressure to enhance the electrical contact between the particles (Figure 1c). The heat and the pressure-induced in this step also improve the packing density of the printed pattern, leading to a highly packed microstructure with enhanced mechanical and electrical properties. To the best of our knowledge, this is the first demonstration of bimodal biodegradable ZnMPs and ZnNPs (ZnMPNPs) conductive paste with a simple low-temperature heat pressure sintering process for use in flexible PTB devices. As a proof-of-concept, the technology was used to fabricate a flexible wearable wireless printed heater for control and on-demand delivery of antibiotics into infected wounds. The low cost and biocompatibility of the materials and the simple post-printing sintering process demonstrate that the newly developed conductive ZnMPNPs paste holds considerable promise for a wide range of future paper-based sensors and actuators for different healthcare and food safety applications.

#### 2. Results and Discussion

To prevent bubbles and microcracks formation, it is important to effectively dry the solvents from printed traces before the heat

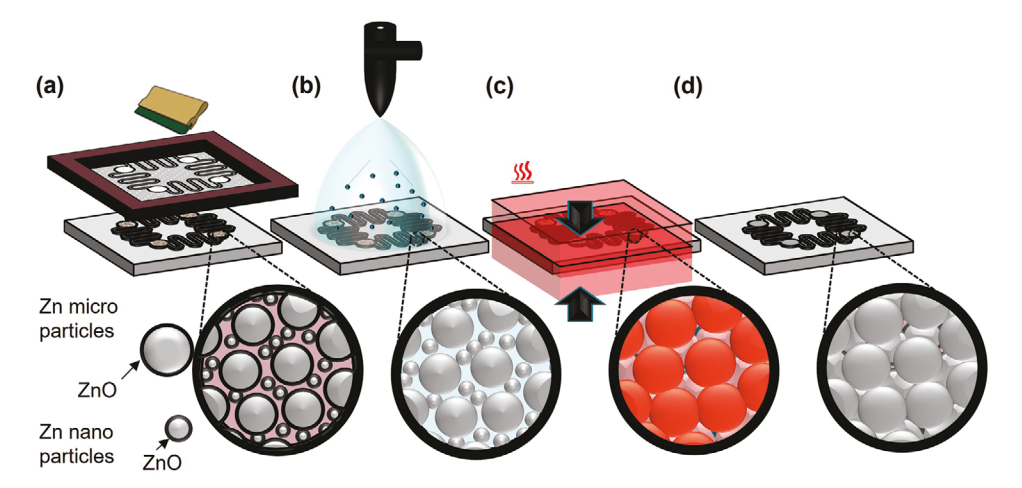


**Figure 1.** Schematic of printing and sintering process of bioresorbable bimodal conductive ZnMPNPs paste. a) Screen printing of ZnMPNPs trace. b) Acetic acid spraying and removal of oxide from Zn particles surfaces. c) Heat press sintering of printed trace. d) Final sintered trace with enhanced packing density and high conductivity.

www.advancedsciencenews.com www.advmattechnol.de



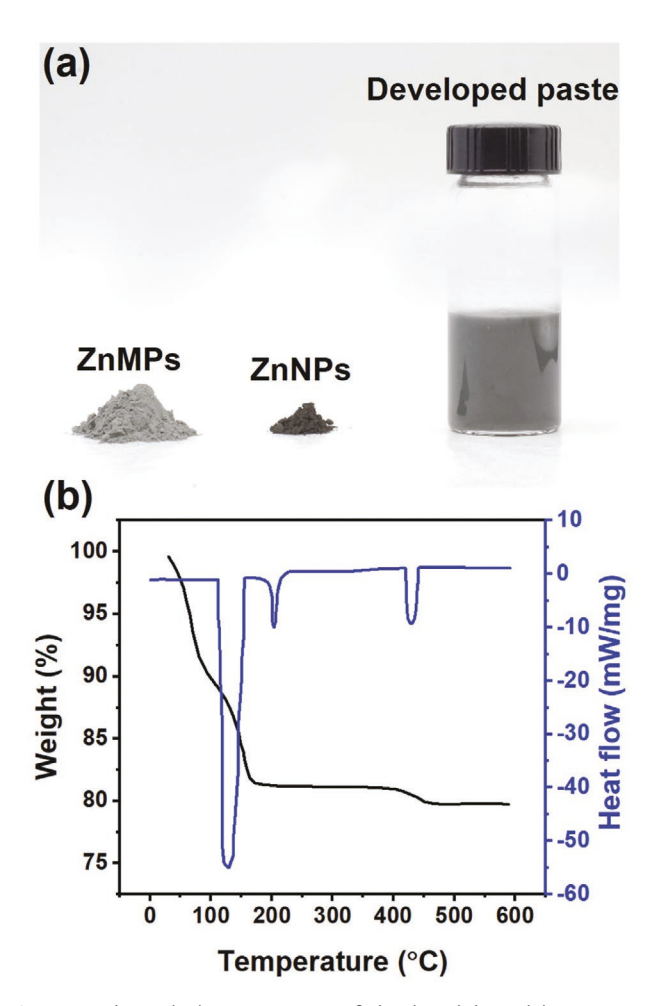


**Figure 2.** Thermal characterization of developed bimodal ZnMPNPs paste. a) ZnMP and ZnNP powder and the final paste. b) TGA and DSC analysis of the ZnMPNPs paste.

press sintering process. To identify the drying kinetics of the ZnMPNPs paste, a differential scanning calorimetry (DSC) and thermogravimetric analysis (TGA) were performed, Figure 2. The TGA analysis demonstrated a primary weight loss occurring in the range of 30.21 to 155.41 °C that corresponded to the evaporation of the solvent. The strong endothermic peak in the DSC graph confirmed that most of the solvent could be removed with a drying temperature of around 128.73 °C. The second endothermic peak in the DSC curve at 203.1 °C was attributed to the degradation of EG (used as a secondary heat-activated reducing agent in the paste preparation). Finally, a third endothermic peak corresponding to the decomposition of the PVP binder was observed at 429.43 °C, which resulted in a total weight reduction of about 2% at 451 °C. At this temperature, the total weight loss of the printed trace was 20% which corresponded to the total weight percentage of the conductive filler used in the bimodal paste preparation. These results revealed that the wet printed trace would require a temperature of at least 128 °C to remove the solvent from the printed traces effectively. Therefore, all printed traces were dried in a hot air oven set at 128 °C for 10 min before the heat pressure sintering process.

Figure 3 demonstrates the result of sheet resistance assessment of acid-treated ZnMPs and ZnMPNPs (with 20 wt% of

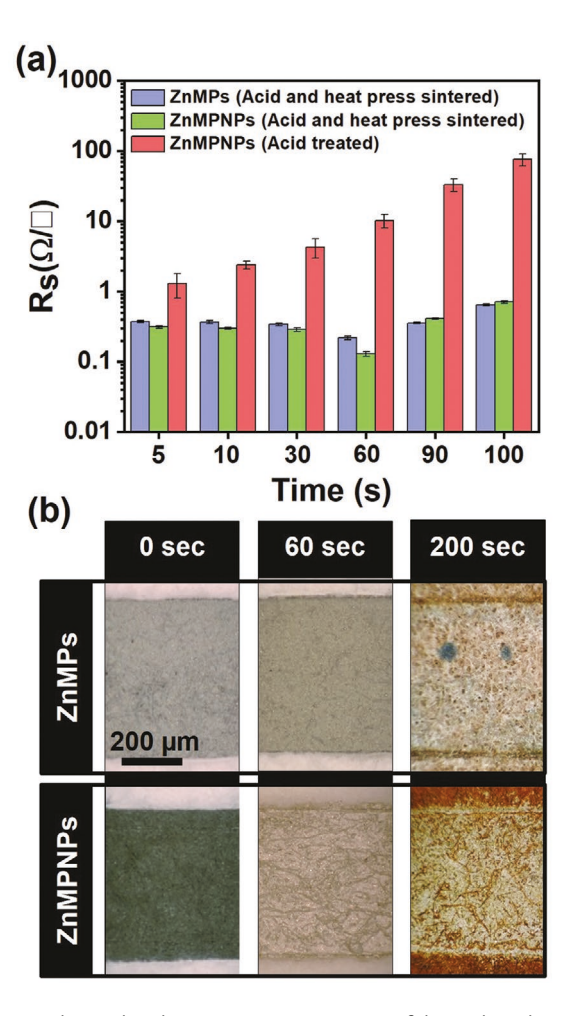


**Figure 3.** Electrical and microscopic assessment of the Zn-based printed traces. a) Sheet resistance measurements of ZnMPs printed trace after heat press sintering with different durations and ZnMPNPs printed trace before and after heat press sintering with different durations. b) Microscope images of printed traces heat press sintered with different durations.

ZnNPs) printed trace before and after heat press sintering at 220 °C with different durations and ZnMPNPs printed traces that was acid-treated without the heat press process as a control. This analysis showed a strong dependence on the electrical resistance of the final traces with different durations of heat press. The ZnMPNPs printed traces without the heat press process showed unstable electrical resistance with a gradual increase over time caused by the slow reoxidation of the ZnMPs and ZnNPs in the printed trace. The lowest electrical resistance was achieved with the heat press duration of 60 s. The ZnMPNPs traces with the optimum heat press sintering process on average showed (0.13  $\Omega$   $\square^{-1}$ ) close to half of the sheet resistance of sintered ZnMPs (0.22  $\Omega$   $\square$ <sup>-1</sup>) traces with the final thickness of 15 µm (Figure 3a). Longer durations of heat press resulted in an overall increase in resistance which is explained by the excessive heat, which resulted in damage to the conductive traces caused by burning the paper substrate. The excessive heat could also lead to the PVP binder burning and degradation that resulted in the printed trace poor adhesion to the substrate (Figure S2, Supporting Information).



Therefore, to prevent the printed trace from reoxidation and to remove the unwanted pores from the printed trace microstructure, heat press sintering was performed at the melting point of  $(CH_3COO)_2Zn$  ( $\approx 220$  °C). At this temperature, the simultaneous application of heat and pressure induces extraordinarily improved through-thickness contact between the particles and the final packing density of the printed trace.

The packing efficiency of the printed traces was investigated via 3D confocal microscopy (Figure S1, Supporting Information). The through-thickness profile of the ZnMPs and ZnMPNPs compositions before and after sintering revealed a clear reduction of  $\approx 5.1~\mu m$  for ZnMPNPs composition after heat press sintering with the optimum setting and duration (Figure S1, Supporting Information). This change in thickness was noticeably lower (1.9  $\mu m$ ) in ZnMPs after the heat press sintering process (Figure S1 in Supporting Information).

The microstructure and the packing density of ZnMPs and ZnMPNPs were qualitatively investigated by scanning electron microscopy (SEM) before and after the heat press sintering process.

Surface SEM images of ZnMPs composition, although show signs of welding between the ZnMPs, a large number of pores exist between the particles after this sintering process, **Figure 4**a-b. In contrast, ZnMPNPs show a significantly lower number of pores after heat press sintering, Figure 4c,d. SEM images of the paper substrate showed no sign of thermal damage to the cellulose fibers of the paper substrate after the heat press sintering process with the optimized settings, Figure 4e,f.

To further investigate the quality of the heat press sintering process through the thickness of the ZnMPs and ZnMPNPs printed traces, a cross-sectional SEM analysis was performed

The effect of excessive thermal energy was also reflected in the microscope images of the printed traces with different durations of heat press (Figure 3b). In this set of figures, one can see that the color clearly changes into a bright silverish gray after the heat press sintering of ZnMPNPs with an optimal 60 s duration. However, this color change was less observed in ZnMPs traces (Figure 3b). In general, longer heat press durations resulted in a significant color change in the paper from white to brown for both ZnMPs and ZnMPNPs compositions (Figure 3b).

The obtained results show the necessity of both acetic acid treatment and heat press to achieve minimal electrical resistance in printed ZnMPNPs traces. In this process, the acetic acid (CH $_3$ COOH) reacts with zinc oxide (ZnO) according to the following reaction<sup>[25]</sup>

$$ZnO + 2CH3COOH \rightarrow (CH3COO)2 Zn + H2O$$
 (1)

This reaction results in the dissociation of ZnO formed around Zn particles, followed by the partial welding of the particles together [22] and the formation of a thin layer of  $(CH_3COO)_2Zn$ . After such reaction, although the conductive fillers within the printed feature are welded together segmentally, the porous structure of the pattern after acid treatment prevents further improvement in lowering the sheet resistance of the printed trace by disrupting the formation of the electron pathway throughout the matrix of the printed trace. This partial welding results in the reoxidation of the printed trace composed of ZnMPs and ZnNPs over a short period of time that leads to a more than 70 times increase in the sheet resistance of the printed trace within 70 s of exposure to room temperature after acid treatment (Figure 3a).

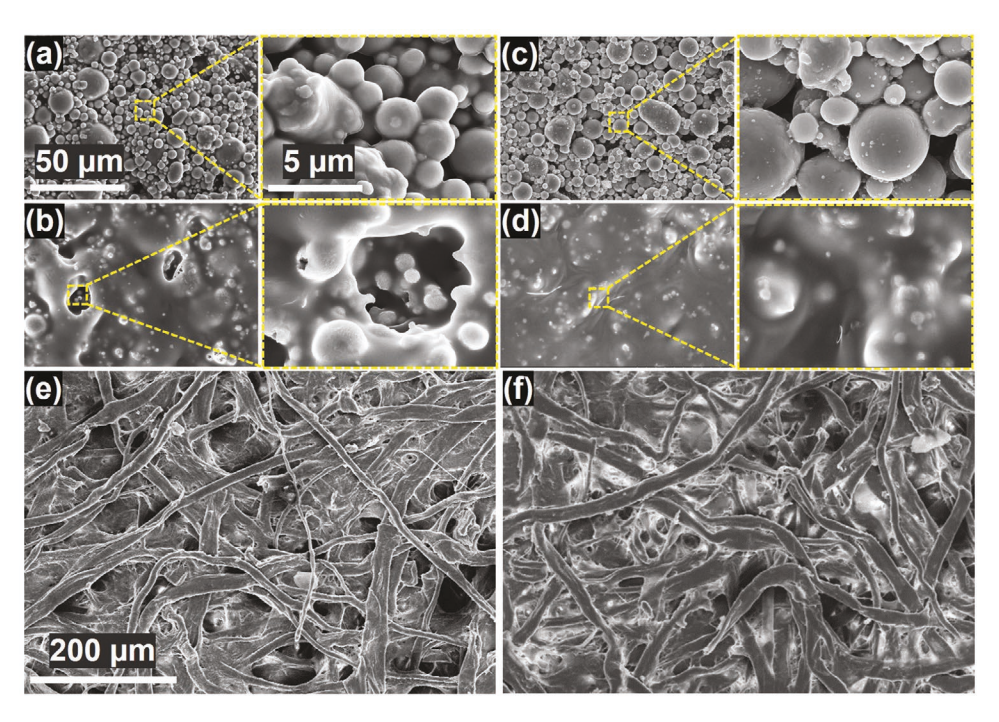
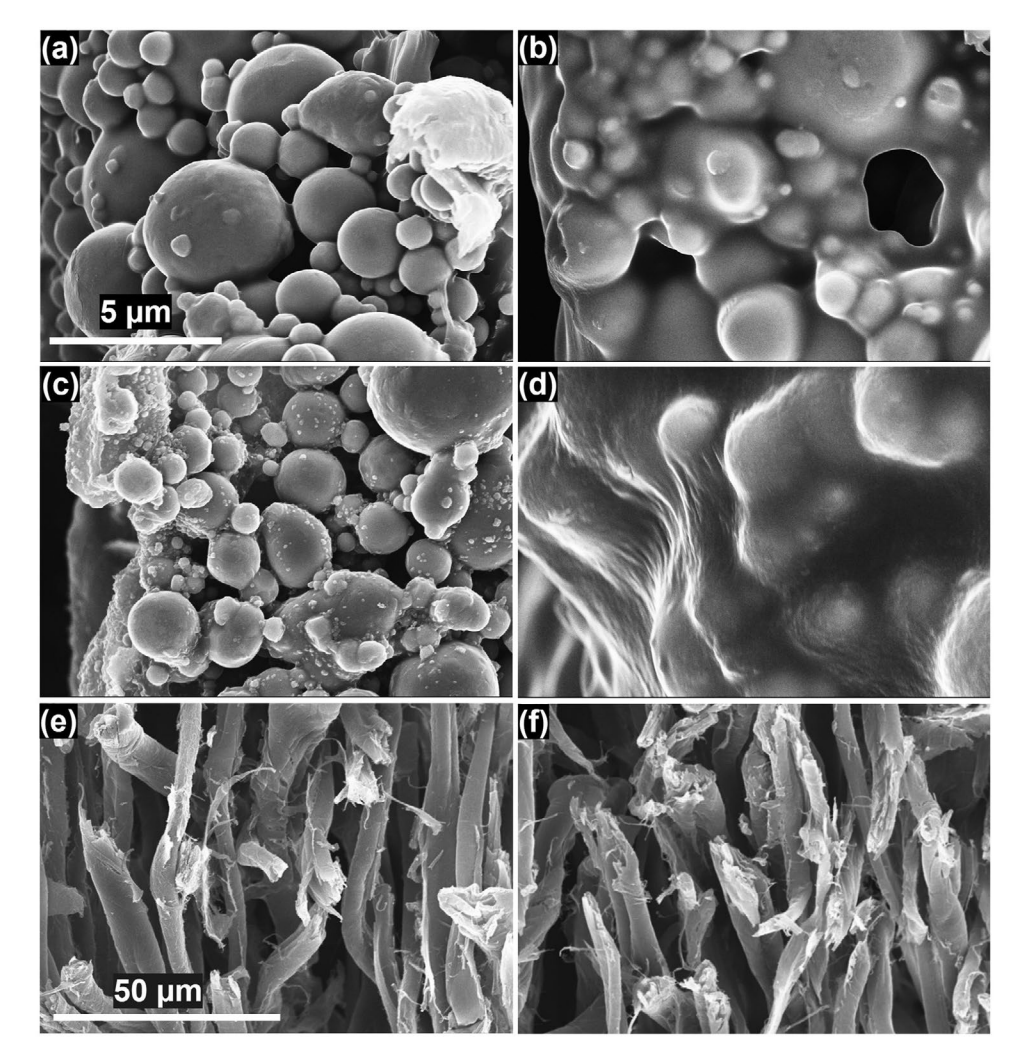


Figure 4. Surface SEM images of printed traces and cellulose paper substrate. ZnMPs composition a) before and b) after heat press sintering. ZnMPNPs composition c) before and d) after heat press sintering. Cellulose paper substrate e) before and f) after heat press sintering.





**Figure 5.** Cross-sectional SEM analysis of printed traces and cellulose paper substrate. ZnMPs composition a) before and b) after heat press sintering. ZnMPNPs composition c) before and d) after heat press sintering. Cellulose paper substrate e) before and f) after heat press sintering.

(Figure 5a-d). Results of this analysis revealed that the welding of particles together is quite dominating due to the sintering mechanism for both compositions through the thickness (Figure 5b,d). Nevertheless, the difference between ZnMPs and ZnMPNPs compositions arises from the fact that only 20 wt% of ZnNPs could fill the pores between the ZnMPs for ZnMPNPs composition and eliminate most of the pores through the thickness of this composition after compaction induced by heat press sintering (Figure 5d). This study provides further rationale for the significantly lower sheet resistance of ZnMPNPs composition (0.13  $\Omega$   $\square^{-1}$ ) compared to that of ZnMPs composition with an optimal sheet resistance of  $0.22 \Omega \square^{-1}$ . We believe that one of the major contributing factors to such low sheet resistance is the perfect adhesion between the cellulose paper substrate and the printed pattern. Such adhesion can only be achieved if the thermal energy applied to the printed pattern by heat press sintering would not induce any damage or defect to the fibrous structure of the paper substrate. Cross-sectional SEM analysis further confirmed no sign of damage induced to the microstructure of the paper after heat press sintering with the optimized duration (Figure 5e,f).

However, common polymeric substrates, such as polyethylene terephthalate (PET) and polyethylene naphthalate (PEN), are incapable of withstanding temperatures as high as 220 °C due to their low glass transition temperature (<120 °C), limiting the application of the developed biodegradable ZnMPNPs paste to circuits and devices on paper substrates.

Figure 6 shows the X-ray diffraction patterns of ZnMPs (Figure 6a) and ZnMPNPs (Figure 6b) before and after heat press sintering. The existence of a small peak at 32° diffraction angle associated with ZnO before heat press sintering for both ZnMPs and ZnMPNPs compositions indicated partial welding of ZnMPs in the paste after acid treatment. This partial welding, which is mainly due to the existence of pores between the particles before heat press sintering, was the main contributing factor for reoxidation of the printed trace for both compositions upon exposure to room temperature after acid treatment. However, a considerably different oxidation behavior was observed once both compositions were heat press sintered with a substantial reduction in the intensity of the ZnO peak. It can be seen from XRD spectra of the ZnMPNPs traces that no noticeable peak associated with ZnO was detected, which

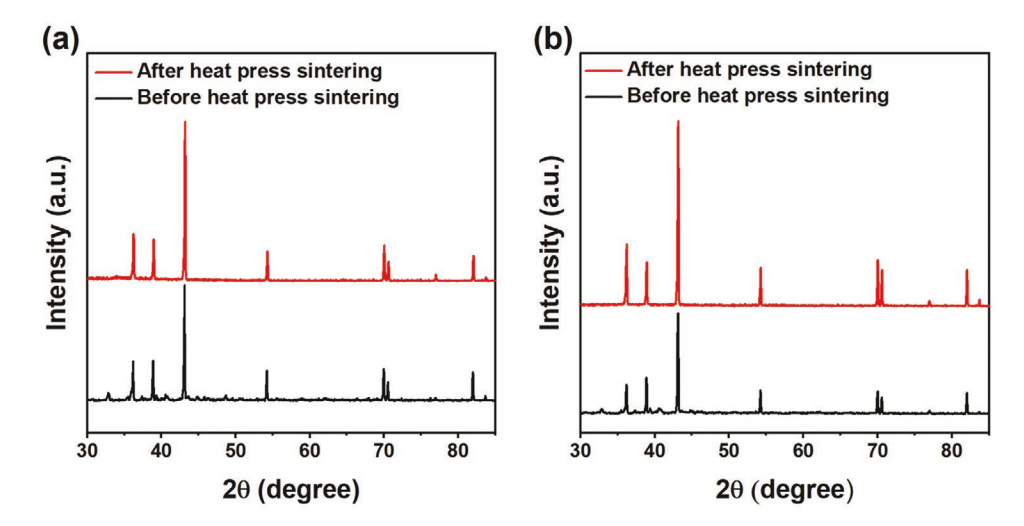


Figure 6. GIXRD spectrum measurement of the acid-treated bimodal paste with compositions of a) ZnMPs and b) ZnMPNPs before and after heat press sintering.

suggests that acid treatment followed by the heat press process effectively removed the oxide compounds from the structure, forming densely packed Zn metal trace. This observation further approves the claim made that the simultaneous acid treatment and heat press sintering significantly contribute to enhanced welding of conductive fillers in both compositions that could prevent reoxidation of Zn particles in the printed trace at the end of the sintering process.

For many PTB applications, the printed circuit requires to maintain highly stable electrical conductivity under a different mechanical deformation. Therefore, the robustness/reliability of the printed Zn traces was assessed under different bending cycles (Figure 7a,b). The electrical resistance of the ZnMPs and ZnMPNPs printed trace with optimized sintering process was continuously measured over cyclic bending, as shown in Figure 7c.

It can be seen that the ZnMPNPs printed trace maintained its initial electrical conductivity up to 13 000 cycles while sharp changes in electrical resistance of ZnMPs printed trace emerged before the 100th cycle (Figure 7c). Surface SEM analysis of ZnMPNPs printed trace showed no signs of surface cracks or delamination after 13 000 cycles of bending (Figure 7d). However, surface microcracks were clearly observed on the surface of ZnMPs printed trace, which explained the sharp increase in electrical resistance (Figure 7e).

Figure 7f,g shows a simple, flexible paper-based circuit lighting with an array of LEDs using developed ZnMPNPs with the optimized sintering process. The results indicated that due to the superior conductivity of the developed paste, only 2.5 V DC voltage could enable simultaneous, visible, and uniform illumination of three LEDs. In addition, the printed pattern with the developed bimodal paste could maintain its uniform light illumination among the three LEDs during mechanical bending load with different bending curvatures (Figure 7h–j), twisting (Figure 7k), and mixed-mode deformation (Figure 7l,m).

In addition to mechanical strength, long-term environmental stability of the obtained optimal sheet resistances at different temperatures and relative humidity is a contributing

factor to enabling the durable performance of PTB for use in food packaging and health monitoring applications. Figure S3, Supporting Information, demonstrates the recorded changes in sheet resistance of ZnMPs and ZnMPNPs printed traces that were exposed to ambient ( $T = 23^{\circ}$ , RH = 40%) and accelerated ( $T = 70^{\circ}$ , RH = 100%) environmental conditions over 7 days. Both ZnMPs and ZnMPNPs composition showed a stable sheet resistance in ambient conditions with minimal changes in the sheet resistance (Figure S3a, Supporting Information). However, when exposed to accelerated conditions, the ZnMPs printed trace sheet resistance value reached more than twice (0.56  $\Omega$   $\square^{-1}$ ) the initial resistance value (0.22  $\Omega$   $\square^{-1}$ ) only after 3 days (Figure S3b, Supporting Information). A further nonlinear increase was observed for the following days up to the maximum of 3.4  $\Omega$   $\square$ <sup>-1</sup> on the 7th day of the measurements, whereas the ZnMPNPs printed trace showed quite a high degree of sheet resistance stability in the accelerated condition during the 7-day period (Figure S3b, Supporting Information). This observation is mainly attributed to the ultrapacked, and uniform microstructure of ZnMPNPs printed trace after heat press sintering that resulted in the removal of pores from the microstructure, which enhances the physical contact between the metal particles and reduces the potential risk of pitting and crevice corrosion in the printed trace.

Recent advancements in the field of printed flexible transient electronics have enabled employing novel technologies and conductive pastes formulations that could be used as a potential wearable drug delivery system with excellent conformal contact with the skin.<sup>[26,27]</sup> Such systems can be used as an active drug delivery platform that could deliver a drug to a targeted site in a controlled manner by external stimulation such as a thermal field with no need for complicated external electrical components.<sup>[28–31]</sup> Some of the benefits of such drug delivery systems are that they could maintain the drug concentration at the targeted site on the tissue for a predefined period, reduce the drug toxicity, and improve the therapeutic efficacy.

Hence, as a proof-of-concept, we have developed a wearable and flexible printed paper-based patch for on-demand delivery of antibiotics into skin wounds using the developed ZnMPNPs

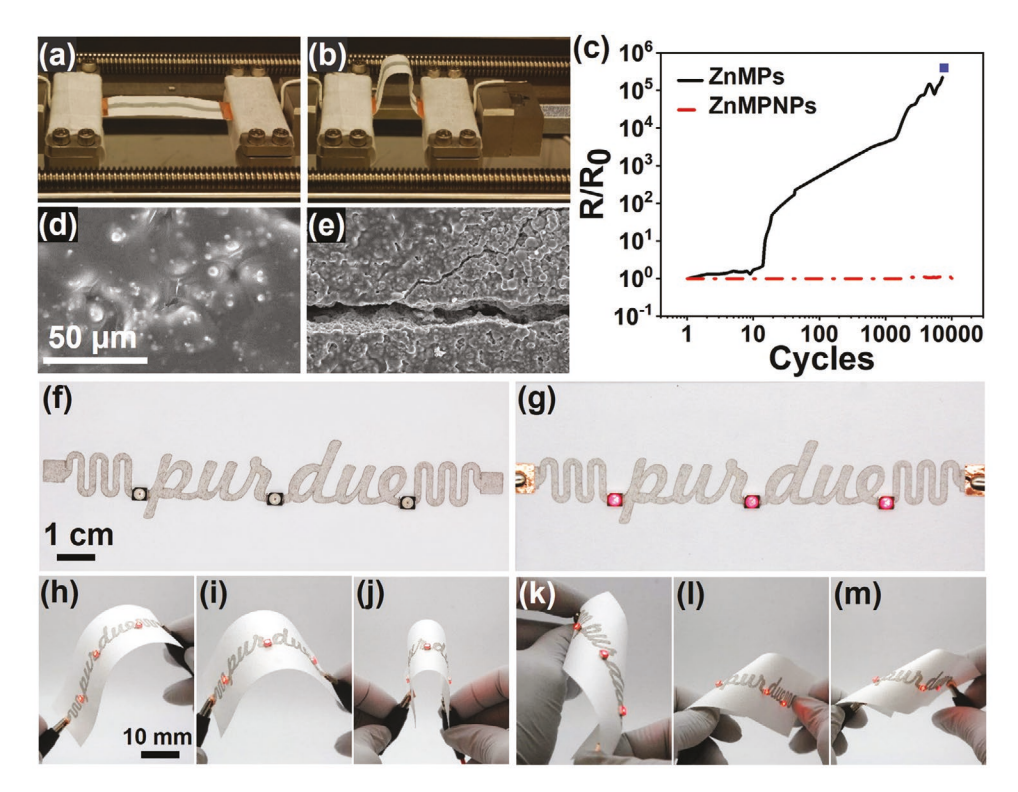


Figure 7. Mechanical and electrical characterization of Zn-based bimodal paste. Photographs of ZnMPNP printed trace a) before and b) after bending. c) Change in the electrical resistance of ZnMPs and ZnMPNPs printed trace under cyclic bending load (square indicates open circuit). SEM images of d) ZnMPNPs and e) ZnMPs printed trace after 13 000 bending cycles. f,g) Images of a simple LED circuit using ZnMPNPs conductive paste with optimized heat press sintering f) before and g) after applying 2.5 V DC to the circuit. h–m) The printed circuit lighting maintained equal illumination among three LEDs under different h–j) bending conditions k) twisting and l,m) mixed-deformation.

conductive paste (Figure 8a). In this design, a thermo-responsive drug releasing system comprising of a polymer composite (PVA and antibiotics) was infused into the fibrous network of the paper substrate containing a printed flexible heater to provide on-demand release of antibiotics into dermal wounds. The heater on the patch is wirelessly powered by an external coil that operates at a frequency of 220 kHz with 2 W power, Figure 8a. The generated alternating magnetic field within the external coil induces an electrical current in the printed coil on the patch. The current passing through the printed circuit results in an overall loss of energy in the form of heat, which elevates the patch temperature and results in the release of antibiotics into the wound.

Figure 8b shows a representative photo of the patch attached to a mannequin hand using a medical transparent waterproof dressing (Nexcare Tegaderm, 3M) and thermal profile on the surface of the patch.

To identify the temperature profile required to trigger the drug release, an experiment was designed where first; the printed patch on the paper was laser cut into circles of diameter of 35 mm and cast with 10 wt% PVA loaded with 0.3 g direct red 80 dye. Direct red 80 dye was chosen as a model drug with the same molecular weight and particle size as the vancomycin antibiotic to evaluate the release and thermal characteristics of the designed patch. Additionally, such red dye provides a fast, simple, and visually observable confirmation of the release phenomenon into the medium. The printed patch was placed

in 1 mL of fresh PBS solution and aligned under the external coil, and the temperature distribution driven by on-off cycles of the patch induced by the external alternating magnetic field was monitored by an IR camera over a period of 3 min at room temperature (25  $^{\circ}$ C).

Figure 8c shows a series of images captured through an IR camera during the on and off cycles of the printed patch that alternate between heating up and cooling down for 3 min. A symmetrical temperature distribution along the length of the printed patch was observed. The thermal analysis of heat maps obtained from IR imaging revealed that at least 2 min of wireless power-up was needed to increase the average temperature along the length of the patch to  $\approx 60$  °C (Figure 8d,f). This level of temperature was needed to initiate the dissolution of a fully hydrolyzed PVA-loaded dye matrix leading to the mobilization of the dye entrapped in the PVA matrix. At this temperature, the diffusion of the dye through the paper started, which led to the release of the dye into the PBS solution.

Figure 8f demonstrates that further increase in heat activation time to beyond 2 min resulted in stable temperature distribution. A similar trend was observed during the off-cycle of the printed patch, where the temperature distribution along the length of the patch was monitored during 3 min powered-off period. It can be seen from Figure 8e that the off-cycle temperature variations displayed a similar symmetrical distribution along the length of the patch. In addition, a minimum

www.advancedsciencenews.com www.advmattechnol.de

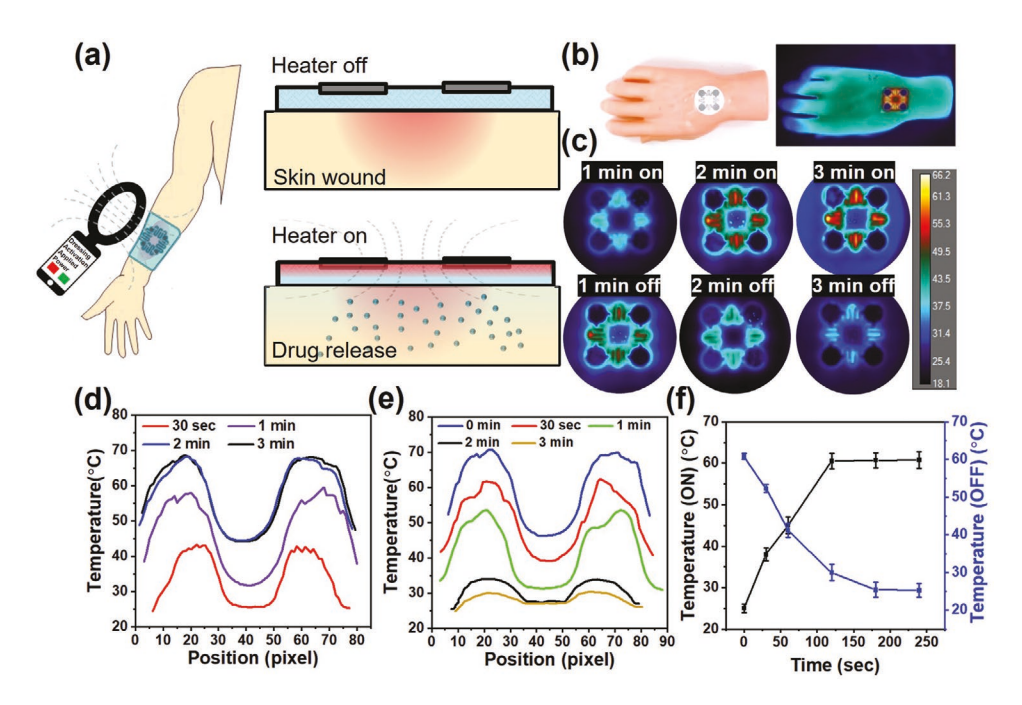


Figure 8. Printed paper-based wireless heater for wearable on-demand drug delivery. a) Illustration of wireless drug delivery by the printed ZnMPNPs heater onto the skin wound. b—f) Thermal characterization of the optimally sintered printed ZnMPNPs heater via infrared imaging. b) Photographs of the wireless printed heater attached to a plastic mannequin hand and corresponding thermal heat map after wireless heating. c) Thermal heat maps of the wireless heater during 3 min on-off cycle. The temperature profile of wireless heater during d) 30 s to 3 min on cycle and e) 3 min off cycle. f) The average temperature change of the wireless heater over the effective patch release area in response to different durations of thermal stimulation by the primary coil.

of 3 min was required for the average temperature along the length of the patch to reach back to room temperature (Figure 8e). Although it has been reported that thermal stimulation is harmless for epidermal drug delivery, [32] increasing the temperature of the skin to more than 45 °C range could be potentially damaging to the skin. [33–35] Therefore, to minimize any type of damage to the skin surface, the paper-based delivery platform was printed on a thick filter paper substrate (180  $\mu m$  thickness) to minimize any potential heat transfer to the skin by the printed heater.

To understand the drug release characteristics of the designed patch, a systematic study was performed with a phantom dye (Direct red 80) into the PBS medium. **Figure 9**a shows the release profile of the dye from the patch under continuous wireless activation over the course of 27 min. It can be seen that the dye release initiated after 2 min wireless activation and heating up the patch to around 60 °C. A sustained and controlled release profile with 67% cumulative release from the patch can be seen over a period of 22.5 min, beyond which no further release was observed (Figure 9a).

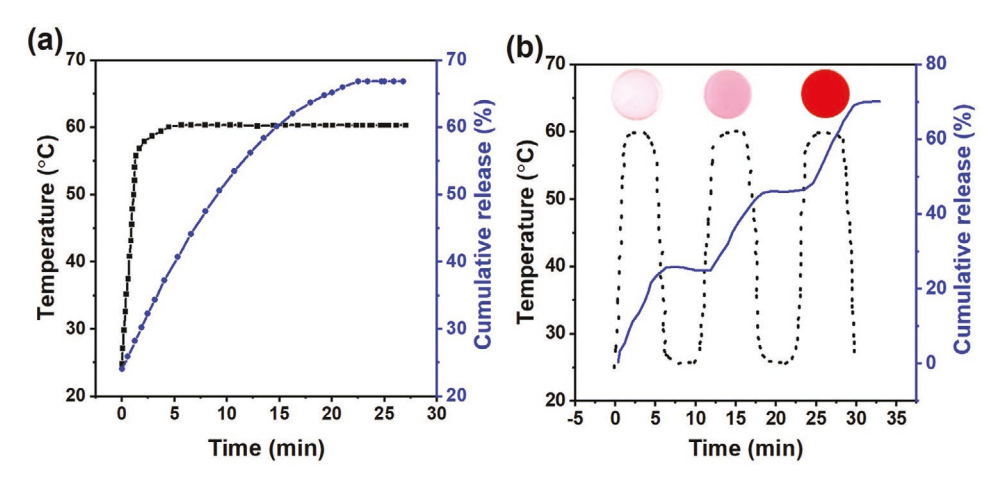


Figure 9. In vitro drug release kinetics from the paper-based patch with printed wireless heater. a) Drug release and temperature profile under continuous wireless activation. b) Cumulative drug release and temperature profile under cyclic activation. Inset: Photographs of change in color of the test medium after different cycles of activating the patch and release of the phantom drug (Direct red 80 dye).

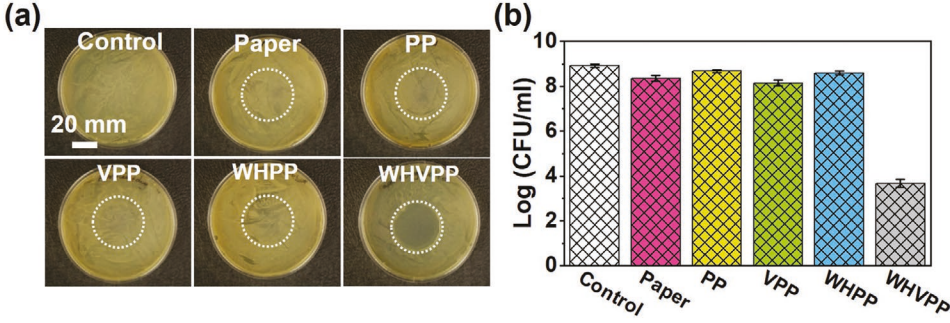


Figure 10. Qualitative and quantitative antibacterial assessment of paper-based patch against S. aureus. a) Zone of inhibition study after 24 h incubation. b) Bacteria quantification (CFU mL-1) of S. aureus. PP: Printed patch, VPP: Vancomycin loaded printed patch, WHPP: Wirelessly heated printed patch, WHVPP: Wirelessly heated vancomycin loaded printed patch.

One of the critical characteristics of active and controlled drug delivery systems that could be used in real clinical applications is the potential to perform dosage of delivery over the course of treatment. Figure 9b shows the performed on-off cycle temperature profile and the corresponding dye release profile. After the first cycle, 23% of the dye was released over a 5 min period from the patch with no further release for approximately 5 more min until the temperature of the patch reached 60 °C in the second cycle. In this cycle, approximately 50% of the dye was released over 25 min (Figure 9b inset). A similar trend as in the first cycle was observed in the second cycle, where the increasing release profile slope was followed by a ≈5 min no-release period. Subjecting the patch to the third cycle resulted in an overall ≈65% release of the red dye into the PBS environment and changed the color of the solution to red (Figure 9b inset).

One of the major challenges of active drug delivery to the wounded regions is to effectively control and limit bacterial infection. It has been reported that in the US alone, chronic wound treatment costs could go up to \$25 billion annually. affecting up to 6 million of the US population.[36] Healing of chronic wounds might take several months and, depending on the condition of the wound, would often require the controlled release of the antibiotic at the specific dosage and time points.[37,38] If not treated properly, some pathogenic strains of bacteria, such as Staphylococcus aureus (S. aureus), could severely inhibit the process of wound healing by biofilm formation, which acts as a physical barrier and limits the penetration of drugs into the wound site.<sup>[38–40]</sup> Here we investigated the possibility of utilizing the developed paper-based wireless drug delivery platform for controlled and on-demand delivery of antibiotics (vancomycin) and eradicating S. aureus by using zone of inhibition (ZOI) and antibacterial efficacy test via colonyforming units (CFU mL<sup>-1</sup>) studies (Figure 10 and Figure S4, Supporting Information).

Figure 10a shows the results of the ZOI study. Among all the test samples, the wirelessly activated paper-based delivery platform containing antibiotics had a noticeable circular ZOI with 34 mm diameter, including the diameter of the patch that resulted from thermal diffusion of antibiotics into the agar plate. No ZOI was observed in TSB plates exposed to test samples, including inactivated printed patches with and without antibiotics, activated printed patches without antibiotics, control, and pristine paper substrate. These observations prove that the observed ZOI is only due to diffusion of antibiotics into the agar plate during the 2 min wireless activation of the patch, and other conditions did not provide any antibacterial effect (Figure 10a).

To quantitively assess the antibacterial efficacy of the printed patch against S. aureus, test samples including inactivated printed patches with and without antibiotics, activated printed patches with and without antibiotic, control, and pristine paper substrate were fully immersed in S. aureus culture medium for 24 h. Figure 10b shows the Log (CFU mL-1) obtained for different samples. It can be seen that among mentioned samples, only activated printed patch with vancomycin antibiotic demonstrated a significantly reduced Log (CFU mL-1) to 3.6 (Figure 10b). These results attribute to the successful eradication of S. aureus by the activated patch upon release of the antibiotic into the culture medium.

To minimize the health-associated risks stemming from the toxicity of a medical device and environmental footprint, one needs to ensure that the device has an appropriate degradation period after their task is completed.

To investigate the degradation period of the developed ZnMPNPs paste, in vitro degradation of the printed patch with the optimized sintering process was monitored by weight loss measurements over 12 days in DMEM/F-12 cell culture media. Figure 11 shows the average normalized weight loss of the printed patch in cell culture media as a function of time. A monolithic decrease in the printed patch weight was observed over 12 days with the maximum %weight reduction of 53.64% after full degradation of the printed traces (Figure 11 inset).

To systematically investigate the biocompatibility of the developed material and process for potential and safe use in healthcare applications, an MTT assay was performed.<sup>[8,41]</sup> In this study, sintered ZnMPs and ZnMPNPs were examined for the toxic activity against NIH/3T3 cells over 7 days. The obtained viability percentage of ZnMPs paste was reported to be 95%, 94%, and 95% on days 1, 4, and 7; respectively. Additionally, the viability percentage of ZnMPNPs paste was 90%, 92%, and 91% on days 1, 4, and 7; respectively (Figure 12a). The reported cell culture study and %viability of the ZnMPs and the ZnMPNPs pastes compared to control revealed a promising biocompatibility characteristic of the developed bimodal paste with NIH/3T3 fibroblast.

The obtained biocompatibility was also confirmed with live/dead staining. The cells were stained with calcein-AM

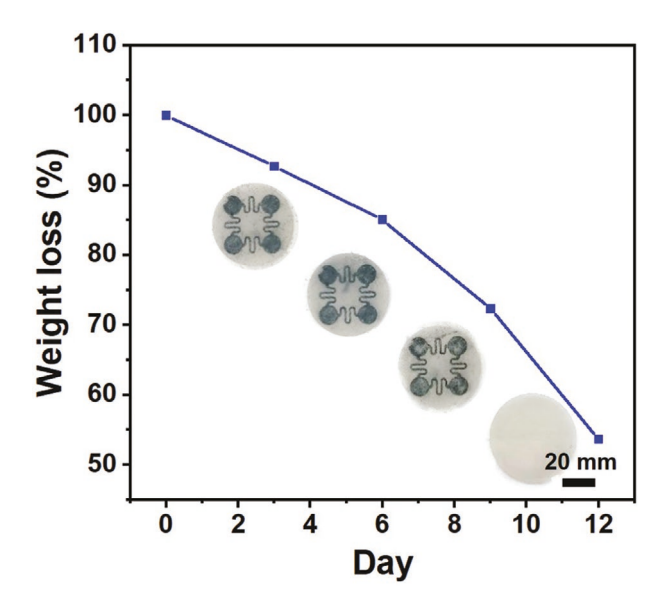


**Figure 11.** Degradation of the wireless heater in DMEM/F-12 cell culture media over 12 days. Weight loss graph of the printed wireless heater over 12 days at different time intervals soaked in DMEM/F-12 cell culture media at 37 °C. Inset: Photographs of the printed patch on paper after soaking in the media for different durations.

(live cells) and ethidium homodimer-1 (dead cells). The cells were labeled green if they were alive and red if they were dead, respectively. The microscopic fluorescence images were observed on days 1 and 7, as shown in Figure 12b. Based on this analysis, the ZnMPNPs showed promising biocompatibility such that there were no dead cells (in red) found on days 1 and 7 of the experiment (Figure 12b), further confirming the biocompatibility of the final ZnMPNPs after the heat press sintering process.

#### 3. Conclusion

This work provides a two-step rapid sintering process for the preparation of a novel bimodal paste composed of ZnMPs

and ZnNPs. Unlike other sintering processes that depend on atomic diffusion, the approach demonstrated here involves the removal of insulating ZnO layer by spray coating acetic acid followed by heat press sintering process to ensure the formation of continuous printed patterns by using conductive ZnNPs. As a proof of concept, the developed paste with optimal sintering conditions was employed to screen-print a wearable wireless heater that exhibited a promising potential to be used as an on-demand localized drug delivery platform. The platform presented in this study paves the way for further development and utilization of paper-based bioresorbable electronics to propose new solutions and techniques for personalized medicine and treating diseases such as chronic skin wounds.

## 4. Experimental Section

Materials: ZnMP (<10 μm diameter) and ZnNP (20 nm diameter) were purchased from Sigma Aldrich and SkySpring Nanomaterials, respectively. Poly(vinylpolypyrrolidone) (PVP) (MW 360000), Ethylene glycol (EG) (anhydrous, 99.8%), ethyl alcohol, pure (anhydrous, ≥99.5%), acetic acid (ReagentPlus, ≥99%), polyvinyl alcohol (PVA) (99% hydrolyzed; MW 8900−98000), Direct Red 80 (Dye content 25%) and vancomycin hydrochloride from Streptomyces Orientalis were purchased from Sigma Aldrich. Gibco Dulbecco's Modified Eagle Medium: Nutrient Mixture F-12 (Ham) (DMEM/F-12) and phosphate-buffered saline (PBS) (Dulbecco's Phosphate Buffered Saline, pH 7.4) were obtained from Thermo Fisher Scientific.

Micro/Nano Paste Preparation: A mixture of ZnMPs and ZnNPs with a weight fraction of 20 wt% ZnNPs was prepared as the conductive filler of the paste. Meanwhile, 0.74 g PVP was dissolved in ethyl alcohol in a separate vial and sonicated for 3 h to obtain a uniform mixture. Then 1 g of EG was added to the PVP solution and sonicated for 1 h. Afterward, 15.4 g of conductive filler was added into the polymer mixture and ultrasonicated for 6 h at 100 W power and 16 kHz frequency (UP400S, Hielscher) to ensure a homogenous dispersion of the particles in the binding matrix. All the materials were of analytical grade and were used as received. The prepared paste was then screen printed on a paper substrate (Grade 1 cellulose filter paper, 180 μm thickness, Whatman) via screen printing (MPS TF-100, Micro Printing Systems). The printing process starts with the sweeping motion of a squeegee made of rubber at 6.66 cm s<sup>-1</sup> velocity across the surface of the screen. The screen was

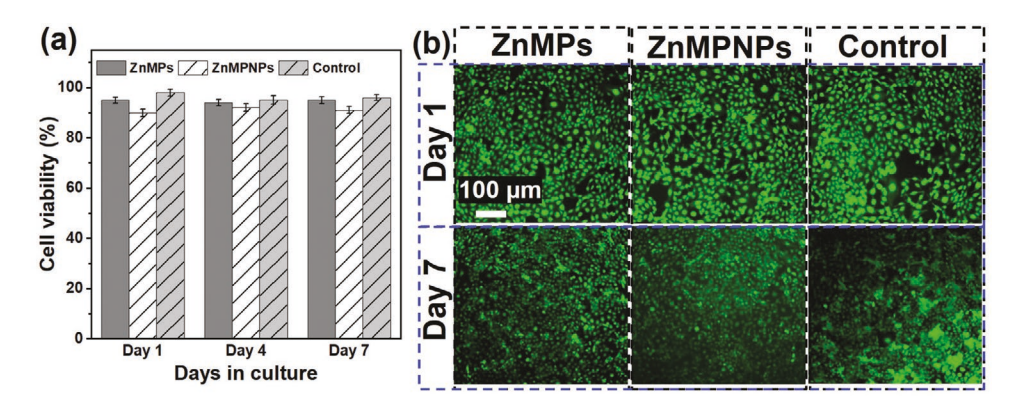


Figure 12. Biocompatibility of ZnMPs, and ZnMPNPs towards NIH/3T3 fibroblast cells. a) Bar graph showing the relative cell viability percentage for ZnMPs, and ZnMPNPs pastes with the MTT assay. b) Immunofluorescence images of NIH/3T3 fibroblast cells on day 1 and day 7 of cell culture along with ZnMPs, and ZnMPNPs coated coverslips. NIH/3T3 fibroblast cells are stained with calcein and ethidium homodimer showing the live (green) and dead (red) cells (n = 3) in three biological replicates. Coverslip without any test material is included as a control. Cell grown on control samples are considered 100% viable and relative viability is calculated.

www.advmattechnol.de

MATERIALS

TECHNOLOGIES

loaded with the prepared paste and placed within 0.1 cm distance from the substrate. Upon squeegee sweeping motion, the paste was flown onto the surface of the substrate, and then momentary contact of the screen to the substrate left the printed traces with rectangular patterns of 3 cm length and 2 mm width. The printed pattern was then dried in a conventional oven at 128 °C for 10 min.

Sintering Process: The printed traces were sintered via acetic acid surface treatment followed by a heat press sintering technique (Digital Power Heat press, Fancierstudio). In this process, a solution of acetic acid and distilled water (1:5 by volume) was sprayed onto a dried printed pattern. The sprayed acetic acid enhances the dissolution of the inherent oxide layer around the Zn particles in the paste and creates a melting pool that facilitates particles packing. Next, the top and bottom plates of the heat press equipment were pre-heated to 220 °C. Before placing the samples between the plates, the plates were closed for 20 s to ensure a steady 220 °C temperature on both plates. Before inserting the samples in a heat press, the top surface and bottom surface of the substrate were protected with parchment paper (Kitchens Parchment Paper Roll, Reynolds) to avoid direct contact of the plates with the printed pattern and the paper substrate. After the insertion of the printed trace between the plates, the pressure was adjusted to 0.6 MPa to ensure maximum compaction of the trace for pore removal within the trace. The printed trace was left between the plates for various time frames in the range from 5 to 100 s. After heat press sintering, the printed traces were removed from the heat press and kept at room temperature for 30 min to cool down. The sheet resistances of printed traces with ZnMPs and ZnMPNPs compositions were calculated according to the following equation

$$\rho_{s} = \frac{R \times W}{L} \tag{2}$$

Where R is the resistance recorded via the four-probe technique (34401A, Agilent), W is the width of the trace, and L is the length of the printed pattern.

Material Properties Characterization: The drying temperature of the paste was investigated via DSC (214 Polyma, Netzsch) and TGA (TG 209 F3 Tarsus, Netzsch) with 20 °C min $^{-1}$  constant heating rate. Optical microscopy (Stemi 2000-c, Zeiss) and field emission SEM (Hitachi S-4800) were employed to assess the surface and cross-sectional microstructure of the printed traces before and after sintering. Grazing incidence X-ray diffraction (GIXRD) characterization was carried out to investigate the crystalline structure of the printed bimodal paste before and after acetic acid treatment and heat press sintering using PANalytical Empyrean multipurpose diffractometer (PANalytical, Almelo, The Netherlands) with a fixed Cu Kα anode ( $\lambda$  = 1.541, 87 Å) operating at 45 kV and 40 mA with an incident beam angle fixed at  $\omega$  = 2°. The thickness profile and 3D topography of the ZnMPs and ZnMPNPs samples were studied by 3D confocal microscopy at 10× magnification (Leica DCM8 Dual Core Measuring Microscope, Leica Microsystems).

The electrical stability of the printed traces was studied by exposing them to two different environmental conditions. The stability assessment tests were performed in an environmental chamber with adjustable temperature, and relative humidity (RH) where the samples of ZnMP and ZnMPNPs printed traces optimally sintered were exposed to ambient ( $T = 23^{\circ}$ , RH = 40%) and accelerated ( $T = 70^{\circ}$ , RH = 100%) environmental conditions. The sheet resistance of the exposed printed traces was monitored over the course of 7 days every 24 h.

Mechanical Characterization: The mechanical durability and flexibility of the printed traces after sintering were evaluated via a bending fatigue test (eXpert4000, Admet) that bends the surface of the trace to a convex shape. Prior to the bending test, ZnMPs and ZnMPNPs sintered traces were printed in 3 mm width and 9 cm length with two ends of the traces adhered with copper tapes soldered with two pieces of 2 cm long copper wires to ensure appropriate ohmic contact. The cyclic bending fatigue tests were performed for a total of 13 000 cycles with a cyclic motion frequency of 15 cycles per min. During the test, the relative electrical resistance change per cycle was recorded in situ

using a digital multimeter (34401A, Agilent) via four-probe technique and the microstructure of the printed traces was investigated after 13 000 cycles via SEM.

The effect of binder (PVP) on adhesion properties of the developed paste was assessed via standard peel tape test by a pressure-sensitive tape (Scotch 898, 3M). Two sets of ZnMPNPs traces were printed on Kapton (polyimide, Dupont) and then heat pressed at two different temperatures of 220 °C (optimal sintering temperature) and 430 °C (above PVP degradation temperature). Then, the tape was cut into a rectangle of size 40 mm  $\times$  19 mm and the sticky side of the tape was ensured, the tape was peeled off at a 90-degree angle at a constant rate manually and the surface of the printed trace and the peeled tape were observed optically.

The degradation of the developed bimodal ZnMPNPs paste was assessed through weight loss measurements and optical disintegration study. For this purpose, a printed heater patch on the paper substrate was laser cut to form a circle of diameter of 35 mm and placed in a polystyrene petri dish that contains 5 mL of DMEM/F-12 cell culture media that was kept inside an orbital incubated shaker (MaxQ 4450, Thermo Fisher Scientific) at 37 °C with 100 rpm speed. Weight loss measurements of the printed sample with ZnMPNPs bimodal paste were performed every 3 days over a period of 12 days. For each measurement, the sample was taken out from the cell culture media, vacuum dried, and weighed with a digital scale (Mettler Toledo, ME 104E) in triplicate. A digital camera was used to monitor the physical degradation of the printed patch for the 12-day period.

Drug Release Studies: PVA was dissolved in deionized water overnight at 80  $^{\circ}\text{C}$  to form a homogenous solution with a 10 wt% ratio. Then 20 g of the prepared solution was mixed with 0.3 g of the dye and allowed to stir for 2 h. Then, 20 µL of the dye mixed solution was drop cast onto the surface of the printed patch laser cut into a circle with 35 mm diameter evenly and placed in the oven at 40 °C for 5 h to ensure solvent evaporation and film formation. The paper patch contacting PVA loaded dye was placed in a Petri dish containing freshly prepared 1 mL of PBS and placed under the external coil at room temperature. The external coil turn-on resulted in the generation of Joule heating in the printed patch that resulted in a temperature rise-up in the printed patch. During this period, the temperature of the printed patch was monitored by an infrared (IR) camera (FLIR A35, FLIR Systems). The amount of dye released in the PBS solution was obtained from an absorption analysis (CLARIOstar Plus, BMG LABTECH). The percent cumulative drug release was obtained by a calibration curve which was prepared by measuring the absorbances of known dye concentrations. Each release experiment was repeated in triplicate and the average result was reported.

Antimicrobial Study: The antimicrobial properties of the developed printed patch were determined by the antibacterial efficacy test via colonyforming units (CFU mL-1) count and zone of inhibition (ZOI).[42] S. aureus (ATCC 2593) was cultured overnight in tryptic soy broth (TSB) (Sigma Aldrich) and incubated at 37 °C with shaking. From the stock solution, 5log<sub>10</sub> CFU mL<sup>-1</sup> of bacterial suspension were used to determine the antimicrobial properties. Six sets of UV sterilized test samples, including inactivated printed patches with and without antibiotics, activated printed patches with and without antibiotic, control, and pristine paper substrate, were housed in six-well tissue culture plates. Each well was inoculated with 1 mL of  $5\log_{10}$  CFU mL $^{-1}$  from the overnight bacterial suspension and incubated at 37 °C. After 24 h, 20 µL was withdrawn and transferred to TSB agar plates after serial dilution. The plates were incubated at 37  $^{\circ}\text{C}$ for 16 h and all the experiments were done in triplicates to determine the average CFU mL<sup>-1</sup>. To determine the ZOI, 100 µL of bacterial suspension was spread on TSB agar plates and then exposed to UV sterilized test samples, including inactivated printed patches with and without antibiotics, activated printed patches with and without antibiotics, control, and pristine paper substrate. Afterward, the test samples were incubated at 37 °C for 24 h and then visually inspected to determine the ZOI.

Biocompatibility Study: MTT assay: Optimally heat press sintered ZnMPNPs and ZnMPs pastes were analyzed for cytocompatibility with

www.advancedsciencenews.com www.advmattechnol.de

ADVANCED MATERIALS
TECHNOLOGIES

NIH/3T3 fibroblast cells by an enzyme-driven colorimetric assay, CellTiter 96 Aqueous One (Promega). The enzyme uses ATP to drive enzyme function, so only live cells convert the substrate into the compound detectable in the spectrophotometer. The samples were cultured with NIH/3T3 cells in DMEM/F-12 media with 10% FBS and 1% Pen/Strep media. To test the cytocompatibility, 12 well cell culture plate was seeded with 200 µl of DMEM/F-12 media with 10% FBS and 1% Pen/Strep containing 5000 cells mL<sup>-1</sup> suspension. Test surfaces seeded with fibroblasts were cultured in a humidified 5% CO2 incubator at 37 °C for 24 h. The cells without the addition of any particles were used as a control. Three identical plates were prepared for ZnMPs, ZnMPNPs, and control. After days 1, 4, and 7 of treatment, DMEM suspension was aspirated from the test wells and covered with 200 uL of MTT reagent. The reagent to media ratio was 20:100  $\mu$ L for a total of 200  $\mu$ L to cover the samples. Samples attached with NIH/3T3 cells were allowed to reduce the substrate for 1 h. Then, three aliquots of 100 µL were transferred to a 96 well plate. The optical absorbance of the samples was read at a fixed wavelength of 490 nm in the spectrophotometer (SpectraMax M2, MolecularDevices, USA), which was calibrated with a blank MTT reagent.

Live/Dead assay: Live/Dead imaging was performed to study the cell viability of the developed paste. The NIH/3T3 fibroblast cells were grown over the conductive sintered pastes. The cells were imaged for live/dead using calcein-AM and ethidium homodimer-1 at different time intervals such as day 1 and day 7. The NIH/3T3 cells were grown as mentioned in the MTT analysis, and three identical plates along with control (no treatment) were used for the study. The cells were imaged with the respective filters in Nikon Ti2 Eclipse, equipped with a camera under a 10× optical lens using NIS-Elements D software.

# **Supporting Information**

Supporting Information is available from the Wiley Online Library or from the author

## Acknowledgements

The authors thank the staff of the Birck Nanotechnology Center at Purdue University for their technical support. Funding for this project was provided by the Ford Motor Company and the School of Materials Engineering at Purdue University. Z. H. and H. W. acknowledge the support from the U.S. National Science Foundation (DMR-1809520) for the XRD effort.

## **Conflict of Interest**

The authors declare no conflict of interest.

## **Data Availability Statement**

The data that support the findings of this study are available on request from the corresponding author. The data are not publicly available due to privacy or ethical restrictions.

### **Keywords**

biodegradable ZnMPNPs conductive paste, drug delivery, heat press sintering, paper-based bioelectronics, wireless wearable patch

Received: December 29, 2021 Revised: March 11, 2022 Published online:

- J. Perelaer, P. J. Smith, D. Mager, D. Soltman, S. K. Volkman, V. Subramanian, J. G. Korvink, U. S. Schubert, J. Mater. Chem. 2010, 20, 8446.
- [2] A. Kamyshny, S. Magdassi, Small 2014, 10, 3515.
- [3] Y. Khan, A. Thielens, S. Muin, J. Ting, C. Baumbauer, A. C. Arias, Adv. Mater. 2020, 1905279, 1.
- [4] A. Zareei, S. Gopalakrishnan, Z. Mutlu, Z. He, S. Peana, H. Wang, R. Rahimi, ACS Appl. Electron. Mater. 2021, 3, 3352.
- [5] Y. Liu, M. Pharr, G. A. Salvatore, ACS Nano 2017, 11, 9614.
- [6] Y. Xu, B. Sun, Y. Ling, Q. Fei, Z. Chen, X. Li, P. Guo, N. Jeon, S. Goswami, Y. Liao, S. Ding, Q. Yu, J. Lin, G. Huang, Z. Yan, Proc. Natl. Acad. Sci. U. S. A. 2020, 117, 205.
- [7] B. Sun, R. N. McCay, S. Goswami, Y. Xu, C. Zhang, Y. Ling, J. Lin, Z. Yan, Adv. Mater. 2018, 30, 1804327.
- [8] A. Zareei, H. Jiang, S. Chittiboyina, J. Zhou, B. P. Marin, S. A. Lelièvre, R. Rahimi, Lab Chip 2020, 20, 778.
- [9] R. Rahimi, S. Lelievre, A. Zareei, S. Chittiboyina, Ultrasonic device, 17/194,361, 2021.
- [10] B. G.Forti V., C. P. Baldé, R. Kuehr, The Global E-waste Monitor 2020: quantities. flows and the circular economy potent.
- [11] M. Sala, D. Medeiros, D. Chanci, R. V. Martinez, *Nano Energy* **2020**, *78*,
- [12] Y. Lin, D. Gritsenko, Q. Liu, X. Lu, J. Xu, ACS Appl. Mater. Interfaces 2016, 8, 20501.
- [13] D. Tobjörk, R. Österbacka, Adv. Mater. 2011, 23, 1935.
- [14] S. Gopalakrishnan, S. Sedaghat, A. Krishnakumar, Z. He, H. Wang, R. Rahimi, 2022, 2101149.
- [15] H. Li, Y. Zheng, L. Qin, Prog. Nat. Sci.: Mater. Int. 2014, 24, 414.
- [16] Y. Liu, Y. Zheng, X.-H. Chen, J.-A. Yang, H. Pan, D. Chen, L. Wang, J. Zhang, D. Zhu, S. Wu, K. W. K. Yeung, R.-C. Zeng, Y. Han, S. Gua, Adv. Funct. Mater. 2019, 1805402, 1.
- [17] B. Jia, Z. Zhang, X. Qu, W. Lin, Nat. Commun. 2020, 11, 1.
- [18] S. Johnston, M. S. Dargusch, Adv. Healthcare Mater. 2019, 1900408, 1.
- [19] R. Rahimi, S. S. Es-haghi, S. Chittiboyina, Z. Mutlu, S. A. Lelièvre, M. Cakmak, B. Ziaie, Adv. Healthcare Mater. 2018, 1800231, 1.
- [20] Z. L. Wang, J. Phys.: Condens. Matter 2004, 16, R829.
- [21] S. Feng, Z. Tian, J. Wang, S. Cao, D. Kong, Adv. Electron. Mater. 2019, 1800693, 1.
- [22] Y. K. Lee, J. Kim, Y. Kim, J. W. Kwak, Y. Yoon, J. A. Rogers, Adv. Mater. 2017, 1702665, 1.
- [23] B. K. Mahajan, X. Yu, W. Shou, H. Pan, X. Huang, Small 2017, 1700065, 1.
- [24] S. Majee, M. C. F. Karlsson, P. J. Wojcik, A. Sawatdee, M. Y. Mulla, N. u. H. Alvi, P. Dyreklev, V. Beni, D. Nilsson, npj Flexible Electron. 2021, 5, 1.
- [25] X. Zhao, B. Zheng, C. Li, H. Gu, Powder technoldgyechnoldgy 1998, 100, 98.
- [26] G. Tiwari, R. Tiwari, S. Bannerjee, L. Bhati, S. Pandey, P. Pandey, B. Sriwastawa, Int. J. Pharm. Invest. 2012, 2, 2.
- [27] H. Patel, D. R. Panchal, U. Patel, T. Brahmbhatt, M. Suthar, I. Pharm. Sci. Biosci. Res. 2011, 1, 143.
- [28] Z. Lou, L. Wang, K. Jiang, Z. Wei, G. Shen, Mater. Sci. Eng., R 2020, 140, August 2019, p. 100523.
- [29] R. Kolakovic, T. Viitala, P. Ihalainen, N. Genina, J. Peltonen, N. Sandler, Expert Opin. Drug Delivery 2013, 10, 1711.
- [30] A. Kamyshny, S. Magdassi, Chem. Soc. Rev. 2019, 48, 1712.
- [31] L. K. Prasad, H. Smyth, Drug Dev. Ind. Pharm. 2016, 42, 1019.
- [32] N. Annabi, A. Tamayol, J. A. Uquillas, M. Akbari, L. E. Bertassoni, C. Cha, G. Camci-Unal, M. R. Dokmeci, N. A. Peppas, A. Khademhosseini, Adv. Mater. 2014, 85.
- [33] D. P. Otto, M. M. De Villiers, Ther. Delivery 2014, 5, 961.
- [34] F. Akomeah, T. Nazir, G. P. Martin, M. B. Brown, Eur. J. Pharm. Sci. 2004. 21, 337.
- [35] A. Mcconville, J. Atchison, A. Roddy, J. Davis, Sens. Actuators, B 2019, 294, 24.



www.advmattechnol.de

- [36] N. A. Richmond, S. A. Lamel, J. M. Davidson, M. Martins-Green, C. K. Sen, M. Tomic-Canic, A. C. Vivas, L. R. Braun, R. S. Kirsner, Wound Repair Regen 2013, 21, 789.
- [37] G. Han, R. Ceilley, Adv. Ther. 2017, 34, 599.
- [38] J. S. Boateng, K. H. Matthews, H. N. E. Stevens, G. M. Eccleston, J. Pharm. Sci. 2008, 97, 2892.
- [39] I. Pastar, A. G. Nusbaum, J. Gil, S. B. Patel, J. Chen, J. Valdes, O. Stojadinovic, L. R. Plano, M. Tomic-Canic, S. C. Davis, *PLoS One* 2013, 8, 1.
- [40] R. Rahimi, A. Zareei, I. Woodhouse, Oxygen-generating biodegradable surgical mesh, 17/317,829, 2021.
- [41] H. Jiang, N. M. Carter, A. Zareei, S. Nejati, J. F. Waimin, J. S. Chittiboyina, E. E. Niedert, T. Soleimani, S. A. Lelièvre, C. J. Goergen, R. Rahimi, ACS Appl. Bio Mater. 2020, 3, 4012.
- [42] V. Selvamani, A. Zareei, A. Elkashif, M. K. Maruthamuthu, S. Chittiboyina, D. Delisi, Z. Li, L. Cai, V. G. Pol, M. N. Seleem, R. Rahimi, Adv. Mater. Interfaces 2020, 1901890, 1.